Bulletin of Engineering Geology and the Environment (2022) 81: 72
https://doi.org/10.1007/s10064-022-02567-5

ORIGINAL PAPER

Influences of water on the microstructure and mechanical behavior of the Xigeda formation

Xiaodong Fu[1,2] · Yuxiang Du[3,4] · Qian Sheng[1,2] · Zhenping Zhang[5] · Juehao Huang[1,2]

Received: 15 October 2020 / Accepted: 31 December 2021 / Published online: 13 January 2022

Abstract
As a typical hard soil and soft/weak rock, the Xigeda formation is a set of Cenozoic lacustrine semi-rock discontinuously distributed in south-western China. Engineering practice shows that water exerts a significant influence on the mechanical properties of the Xigeda formation. X-ray powder diffraction (XRD), scanning electron microscopy (SEM), and triaxial compression tests were conducted by means of in situ sampling of the Xigeda formation in Zhaizi village along the Jiasha River. The mineral composition and microstructure were determined, the deformation and failure mechanisms were investigated, and influences of the water content on both deformation and strength indices were discussed. The results show that (a) the Xigeda formation has a characteristic weakly cemented structure, which differs from that of soil and rock, and this cemented structure is easily damaged under saturated conditions; (b) with increasing water content, both average modulus and shear strength of the Xigeda formation decrease significantly, and influence of water content on peak strength is much greater than that on residual strength; and (c) in the range of tested conditions ($w = 17.79 \sim 30.83\%$, $\sigma_3 = 200 \sim 800$ kPa), both the peak and residual strengths meet the Mohr–Coulomb criterion. The results can provide an experimental basis and mechanism informing engineering practice in the Xigeda formation.

Keywords Xigeda formation · Water content · Microstructure · Mechanical behavior · Strength

Introduction

Many geological hazards have been induced by those geological materials exhibiting a response intermediate to that of rock and soil (Moon 1993; McCammon 1999; Cecconi and Viggiani 2001; Tommasi et al. 2014). Such geological materials do not strictly obey the principles of either rock or soil mechanics, obscuring the failure mechanism and mechanical parameters while exerting adverse effects on many practical scenarios (Barla et al. 1998; Rotaru 2011; Alonso and Pinyol 2014; Abolmasov et al. 2014; Di Maio et al. 2014; Zimbardo et al. 2018). This problem has attracted much attention among the geo-engineering community and scholars, who describe such geological materials as either hard soils or soft/weak rocks (Vaughan 1993; Zhang and Qu 2000; Zimbardo et al. 2018). These include hard clays and clay-shales, soft sedimentary rocks, weak pyroclastic rocks such as tuff, cemented coarse-grained materials such as weak sandstones, residuals soils, and extremely highly weathered hard rocks (Gens et al. 2005). Four symposia/workshops have been held under the theme "Geotechnics of Hard Soils-Weak Rocks" (Kanji 2014; Picarelli 2015). The first symposium, under the auspices of the International Society for Soil Mechanics and Foundation Engineering, was held in Athens, 1993. In 1998, the Italian Geotechnical Society organized the second international symposium in Naples. The next such event was the 15th European Conference on Soil Mechanics and Geotechnical

✉ Xiaodong Fu
xdfu@whrsm.ac.cn

1 State Key Laboratory of Geomechanics and Geotechnical Engineering, Institute of Rock and Soil Mechanics, Chinese Academy of Sciences, 430071 Wuhan, China

2 School of Engineering Science, University of Chinese Academy of Sciences, 100049 Beijing, China

3 Hubei Key Laboratory of Blasting Engineering, Jianghan University, Wuhan 430056, Hubei, China

4 Hubei (Wuhan) Institute of Explosion Science and Blasting Technology, Jianghan University, Wuhan 430056, Hubei, China

5 School of Architecture and Civil Engineering, Shenyang University of Technology, Shenyang 110870, Liaoning, China

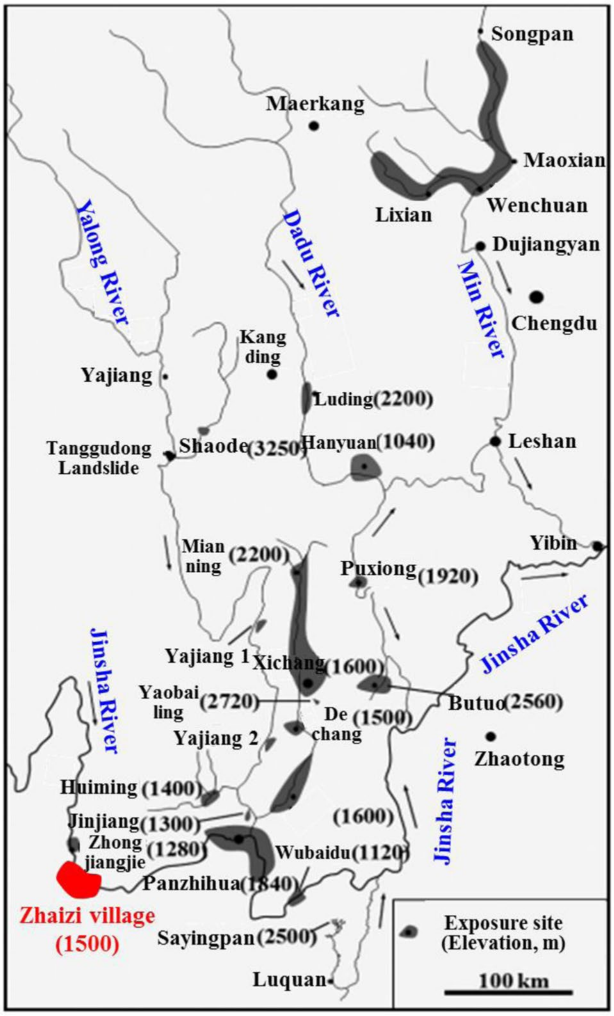

Fig. 1 Distributions of the Xigeda formation. Modified from Xu (2011)

Engineering held in Athens in 2011. In 2013, the Seconda Università di Napoli, the Università di Napoli Federico II, and the Universitat Politechnica de Catalunya jointly organized a Mediterranean Workshop on Landslides entitled "Landslides in Hard Soils and Weak Rocks – An Open Problem for Mediterranean Countries" in Naples. With the efforts of the geo-engineering community and scholars, the mechanical behaviors of some typical hard soils and soft/weak rocks have been extensively investigated (Clayton and Serratrice 1993; Gens and Nova 1993; Tatsuoka and Kohata 1995; Aversa and Evangelista 1998; Shao 1998; Kavvadas and Amorosi 2000; Vukadin 2007; Sitarenios et al. 2011; Hornig and Klapperich 2011; Corominas et al. 2014).

The Xigeda formation is a typical hard soil, soft/weak rock formation. The Xigeda formation is also called the "Huntan formation" but was named with Xigeda (a village in Hongge Township, Yanbian County, Panzhihua City, Sichuan Province) in mind by Yuan in 1958. This formation mainly encompasses fine-grained sandstone, clay, and conglomerate (Zhang 2009). At present, studies of the Xigeda formation mainly include those examining the mechanisms of occurrence, formation age, and mechanical properties. Previous studies attributed the occurrence of the Xigeda formation to either large-scale glacial development in the Pliocene or tectonic deformation that formed a series of lakes (Quaternary Glacier Survey Group 1977; Li et al. 2012). Based on the studies of the Xigeda formation in Xichang City, Luding City, Panzhihua City, and other sites in China, it has been shown that the date of formation is about 1.0 to 4.2 Ma, which is between the Pliocene of the tertiary system and the Pleistocene of the quaternary system (Kong et al. 2009; Xu and Liu 2011).

(a) Jingjiu Twonship of Sichuan Province (Xu, 2011) **(b)** Zhaizi village of Yunnan Province

Fig. 2 Structural characteristics of the Xigeda formation at different sites. **a** Jingjiu Twonship of Sichuan Province (Xu 2011). **b** Zhaizi village of Yunnan Province

Scholars pointed out that water will weaken the physical and mechanical behavior of the Xigeda formation, which may adversely affect its stability (Sun et al. 2012; Ling et al. 2015; Zhou et al. 2017; Wang et al. 2018; Yang et al. 2020).

To investigate the influences of water on mechanical behavior of the Xigeda formation, samples thereof from Zhaizi village, Yunnan Province, China, have been studied. "Field investigation and sampling" presents the field investigation and sampling of the Xigeda formation in Zhaizi village. "Mineral composition and microstructure" analyzes the mineral composition and microstructure of the Xigeda formation by X-ray powder diffraction (XRD) and scanning electron microscopy (SEM). Results of physical and triaxial compression tests are listed in "Measuring the physico-mechanical parameters." In "Influences of the water content on mechanical behavior," influences of the water content on both the deformation and strength indices are discussed.

(a) The site photographed by a drone

(b) Field sampling

Fig. 3 Field investigation and sampling of the Xigeda formation exposed in a foundation pit. **a** The site photographed by a drone. **b** Field sampling

Field investigation and sampling

In south-western China, the Xigeda formation is spread from Songpan County in the north to Zhaizi village in the south and is mainly distributed in bands and flakes with an area of 2.1×10^5 km^2. As shown in Fig. 1, as a set of river–lake facies sediments in quiet water, the Xigeda formation is seen in the valleys of many watersheds across western Sichuan Province and northern Yunnan Province, such as the Jinsha River, the Yalong River, the Dadu River, and the Min River. At different sites, the degree of diagenesis of the Xigeda formation differs; in general, the degree of diagenesis of the Xigeda formation is low and it has the characteristics of rock-like non-rock and soil-like non-soil: geologists refer to this as semi-rock (Liu and Nie 2004). As shown in Fig. 2, the Xigeda formation has an obvious horizontal bedding structure, mainly composed of clay, silt, and silty fine sand (Xu 2011; Xu and Liu 2011).

The Xigeda formation in Zhaizi village along the Jinsha River is a typical deposit caused by a barrier lake. During the construction of the Taoyuan Jinsha River suspension bridge, which forms a key part of the Dali-Yongsheng Expressway, the Xigeda formation is exposed in the foundation pit of the gravity anchorage of the suspension bridge. The foundation pit is in Zhaizi village, Taoyuan Township, Yongsheng County, Lijiang City, Yunnan Province. Figure 3a shows a photograph of the site taken by an aerial drone, the Xigeda formation is located in the south-west foundation pit, and the foundation pit is several hundred meters from the reservoir area of the Ludila Hydropower Station along the Jinsha River. The base elevation of foundation pit is 1229.462 m, and the highest reservoir water level is 1223 to 1225 m. Figure 3b shows the field sampling process, wherein the Xigeda formation is brown/light yellow, medium dense, slightly wet, and mainly composed of silt and sand.

Mineral composition and microstructure

Mineral composition

Three samples of the Xigeda formation were used for XRD analysis. Figure 4 shows the mineral compositions of tested specimens: the results illustrate that the mineral composition of the Xigeda formation is mainly quartz (31 ~ 51%), followed by clay minerals, including illite (11 ~ 38%), montmorillonite (8 ~ 9%), and clinochlore (5 ~ 14%), in addition to small amounts of calcite (8 ~ 12%), albite (0 ~ 12%), and other minerals.

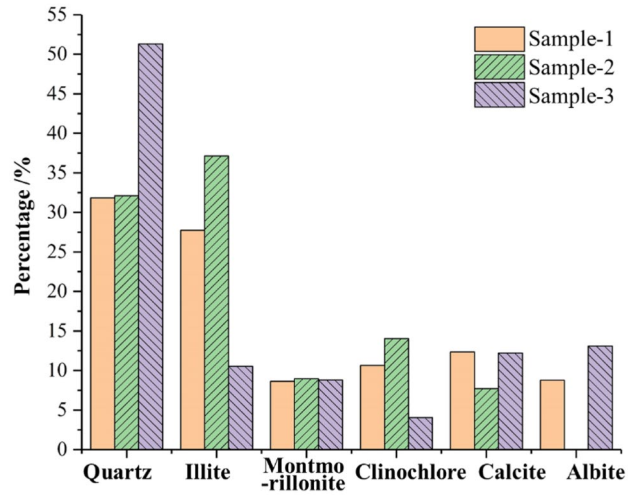

Fig. 4 Mineral compositions

Microstructure of the natural sample

Figure 5 shows the microstructure of a natural specimen as seen by SEM at a water content of 17.79%. It can be observed that the structure is relatively compact; the sample is mainly composed of the silty gravel clasts, the interstitial materials including the matrix and cementing materials. According to the results of the mineral composition assay, the silty gravel clasts are mainly quartz with a particle size of 30 ~ 70 μm, the matrix includes illite, montmorillonite, and clinochlore with a particle size of 5 μm (Fig. 5a). The cementing materials mainly comprise siliceous and clay mineral components. The siliceous cementing materials are present in the form of secondary outgrowth rims growing along the edges of the quartz particles (Fig. 5b); clay mineral cementation could be characterized by a fluffy or acicular structure attached to the particle surface (Fig. 5c).

Comparing the microstructure of the Xigeda formation with that of a silty soil or siltstone, the results show that as shown in Fig. 6a, there are few interstitial materials in silty soil, and the particles are scattered and well-defined; as shown in Fig. 6b, the particles of the siltstone clasts are in either point, line, or inlaid contact with each other; the interstitial materials are dense, and authigenic quartz crystals are fully developed, with authigenic clay minerals on the surface of clastic particles being developed in felt-like or thin-film forms (forming a strong structural bond). However, the specimens sampled from the Xigeda formation have a structure typifying weak compressive cementation, and SEM images show that the microstructure of the Xigeda formation is different from that of the silt soil or the siltstone.

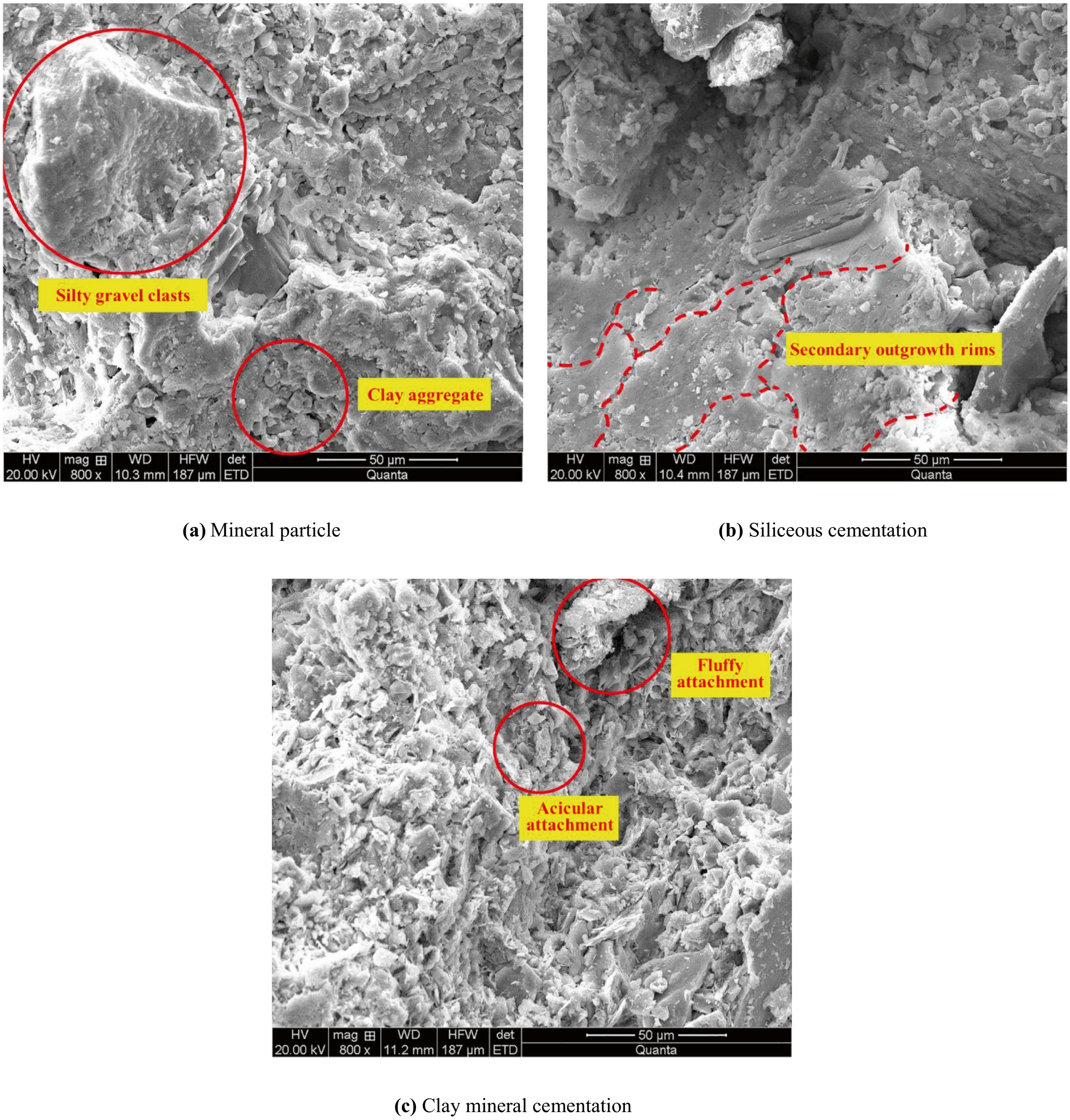

Fig. 5 Microstructure of the Xigeda formation. **a** Mineral particle. **b** Siliceous cementation. **c** Clay mineral cementation

Comparisons of the microstructures of natural and saturated specimens

Figure 7 shows the microstructures of the natural and saturated specimens. Compared to the natural microstructure, the microstructure becomes looser when saturated, the average particle size increases significantly, and the outline of the particle surface tends to be smooth and round, which can be explained from a microscopic perspective. The clay minerals (including the illite and montmorillonite) adsorb the water film, resulting in volumetric expansion and the increased stresses associated therewith: this not only leads to the destruction of the initial cementation structure, but also loosens the entire structure. The increase of particle size is due to the hygroscopic expansion of clay minerals attached to the surface, and the particle surface becomes smooth with disappearance of the fluffy and acicular structures. Due to the molecular force exerted by the water film,

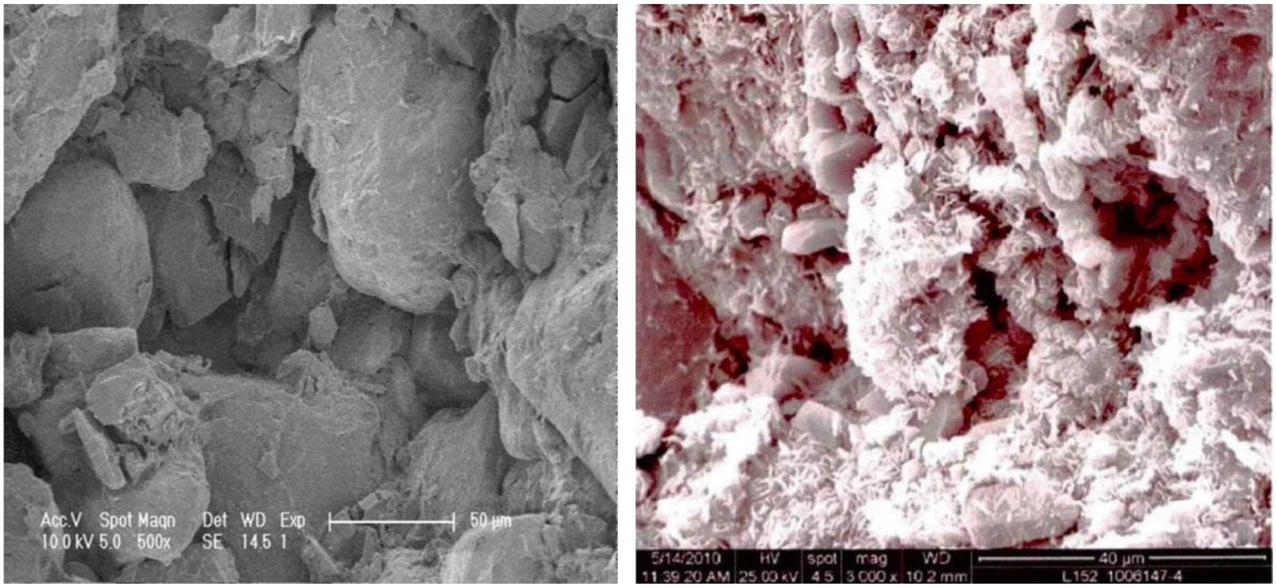

(a) Silty soil (Zhou, 2016) **(b)** Siltstone (Shang, 2012)

Fig. 6 Microstructure of the silty soil and the siltstone. **a** Silty soil (Zhou 2016). **b** Siltstone (Shang 2012)

the clastic mineral particles move from the thicker water film to a thinner water film, showing a tendency to spheroidization; montmorillonite readily slides between the crystal layers after absorbing water, and clastic mineral particles are easily transported in the process of water-film migration, resulting in a rounding of the particle surface. These microscopic failure mechanisms are derived from the chemical reaction between the illite or montmorillonite and the water:

$$K_{0.9}Al_{2.9}Si_{3.1}O_{10}(OH)_2 + nH_2O \rightarrow K_{0.9}Al_{2.9}Si_{3.1}O_{10}(OH)_2 \cdot nH_2O \quad (1)$$

$$(Na, Ca)_{0.33}(Al, Mg)_2Si_4O_{10}(OH)_2 + nH_2O \rightarrow (Na, Ca)_{0.33}(Al, Mg)_2Si_4O_{10}(OH)_2 \cdot nH_2O \quad (2)$$

Measuring the physico-mechanical parameters

Using specimens sampled from the Xigeda formation in Zhaizi village, the basic physical properties were measured (Table 1). To study the mechanical behavior of the Xigeda formation, a series of triaxial compression tests were conducted on cylindrical specimens with a diameter of 39.1 mm and a height of 80 mm.

Five different water contents (17.79%, 20.58%, 24.86%, 26.52%, and 30.83%) were used, the last of which was sufficient to saturate the specimens and the others were obtained from different locations. Figure 8 shows typical specimens with different water contents. For each water content, specimens were tested to failure under four different confining pressures (200 kPa, 400 kPa, 600 kPa, and 800 kPa). During the triaxial loading process, it is noted that the axial load is perpendicular to the horizontal bedding structure of each specimen. The peak and residual strengths under different water contents and confining pressures are summarized in Tables 2 and 3, respectively, where w is the water content, σ_3 denotes the confining pressure, σ_f is the peak strength, and σ_r is the residual strength.

Influences of the water content on mechanical behavior

Stress–strain behavior

According to the results of the triaxial compression tests, the typical stress–strain curve and the failure mode were obtained (Fig. 9). The stress–strain behavior can be divided into five stages: pore/fracture compaction (OA), elastic deformation (AB), unstable fracture (BC), strain softening (CD), and post-fracture (DE).

For each water content, the stress–strain curves of specimens from the Xigeda formation under different confining pressures are illustrated in Fig. 10. The test results show the following:

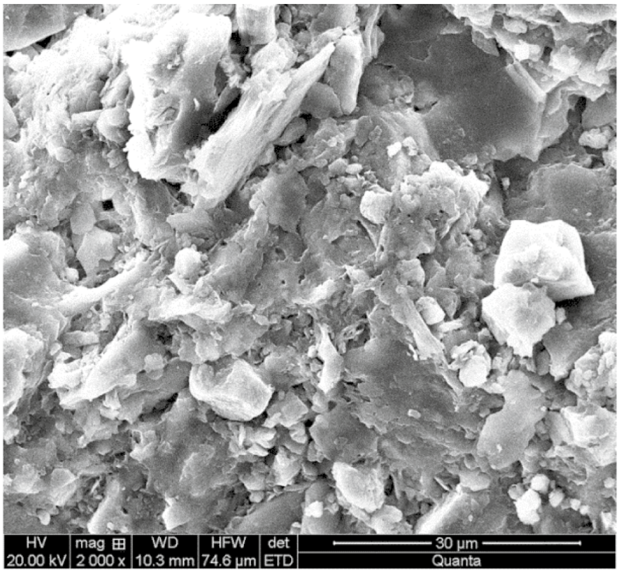

(a) The natural sample

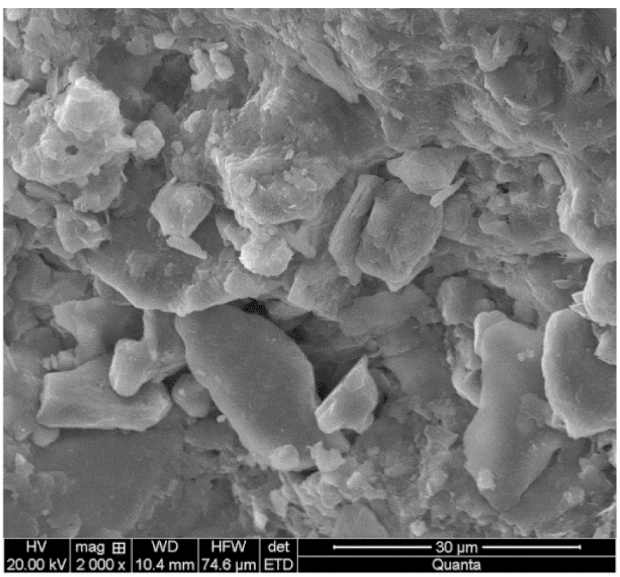

(b) The saturated sample

Fig. 7 Microstructures of different specimens. **a** The natural sample. **b** The saturated sample

(a) Both the peak strength and the residual strength increase with the confining pressure, for example, at a water content of 17.79%, when the confining pressure is increased from 200 to 800 kPa, the peak strength is increased from 711 to 1761 kPa (Table 2), and the residual strength is increased from 413 to 1232 kPa (Table 3).

(b) With increasing confining pressure, the gradients of the stress–strain curves in the elastic deformation stage do not change to any significant extent, while the cumulative strains in the unstable fracture stage increase significantly, and the axial strains corresponding to the peak strengths increase. Table 4 lists the measured axial strains corresponding to the peak strengths, where ε_f is the axial strain. For example, at a water content of 17.79%, when the confining pressure is increased from 200 to 800 kPa, the axial strain corresponding to the peak strength is increased from 0.0103 to 0.0158.

(c) In the strain softening stage, due to the development of fractures in the sample being unstable, the stress–strain curve fluctuates, and this fluctuation becomes more intense with increasing confining pressure.

Under each confining pressure, the stress–strain curves of specimens at different water contents are as shown in Fig. 11. The test results show the following:

(a) When the water content is low, the domain near the peak strength is sharp, and the peak strength drops rapidly to the residual strength, showing the softening characteristics of rock. At a greater water content, the domain near the peak strength is shallower in that the gradient of the stress–strain curve after reaching the peak strength is lower, and the ensuing strain softening becomes less pronounced, typifying the deformation characteristics of soil.

(b) Both the peak strength and the residual strength decrease with increasing water content, and the influence of water content on the peak strength is much greater than that on residual strength. For example, when the confining pressure is 200 kPa, as the water content increases from 17.79 to 30.83%, the peak strength decreases from 711 to 358 kPa (Table 2), while the residual strength is decreased by about half as much from 413 to 295 kPa (Table 3). The peak strength represents the coalescence of the fracture surface/zone, which depends on the cementation of the sample, and this reflects the initial structure of the sample, while the residual strength represents the sliding ability between the upper and lower parts of the fracture surface/zone, which depends on the roughness of the fracture surface/zone or the roundness of mineral particles, and it reflects the structural characteristics of the fracture surface/zone. Thus, it can

Table 1 Basic physical parameters of the Xigeda formation

Parameters	Natural density/(kg/m^3)	Dry density/(kg/m^3)	Water content/(%)	Specific gravity
Range of values	1610 ~ 2000	1370 ~ 1580	17.79 ~ 26.52	2.70 ~ 2.75
Average value	1830	1460	22.44	2.72

Fig. 8 Specimens with different water contents for triaxial compression testing. **a** 17.79%. **b** 20.58%. **c** 24.86%. **d** 26.52%. **e** 30.83%

(a) 17.79% **(b)** 20.58% **(c)** 24.86% **(d)** 26.52% **(e)** 30.83%

Table 2 Peak strengths under different water contents and confining pressures

w/%	σ_f/kPa			
	$\sigma_3 = 200$ kPa	$\sigma_3 = 400$ kPa	$\sigma_3 = 600$ kPa	$\sigma_3 = 800$ kPa
17.79	711.25	1012.80	1453.42	1761.35
20.58	639.21	961.20	1362.19	1620.19
24.86	553.96	879.36	1135.76	1498.16
26.52	479.56	720.32	1036.09	1286.86
30.83	358.41	623.29	834.16	1096.04

Table 3 Residual strengths under different water contents and confining pressures

w/%	σ_r/kPa			
	$\sigma_3 = 200$ kPa	$\sigma_3 = 400$ kPa	$\sigma_3 = 600$ kPa	$\sigma_3 = 800$ kPa
17.79	412.77	708.59	913.41	1232.24
20.58	399.88	645.56	936.24	1156.92
24.86	342.55	568.02	843.49	1056.96
26.52	310.03	573.20	796.57	1018.94
30.83	294.63	544.60	752.56	999.52

be concluded that the ability of the water to weaken the degree of cementation of a specimen is much greater than that of the roughness of the mineral contact surface or changes to the roundness of the mineral particles.

(c) With increasing water content, the gradients of the stress–strain curve in the elastic deformation stage decrease, while the axial strains corresponding to the peak strengths increase. For example, when the confining pressure is 200 kPa, the water content is increased from 17.79 to 30.83%, the gradients of the stress–strain curve in the elastic deformation stage decrease significantly, and the axial strain corresponding to the peak strength increases from 0.0103 to 0.02 (Table 4). This result suggested that the water content exerted a certain influence on both the elastic deformation stage and the unstable fracture stage of the stress–strain curve.

Fig. 9 Typical stress–strain behavior. **a** Stress–strain curve. **b** Failure mode

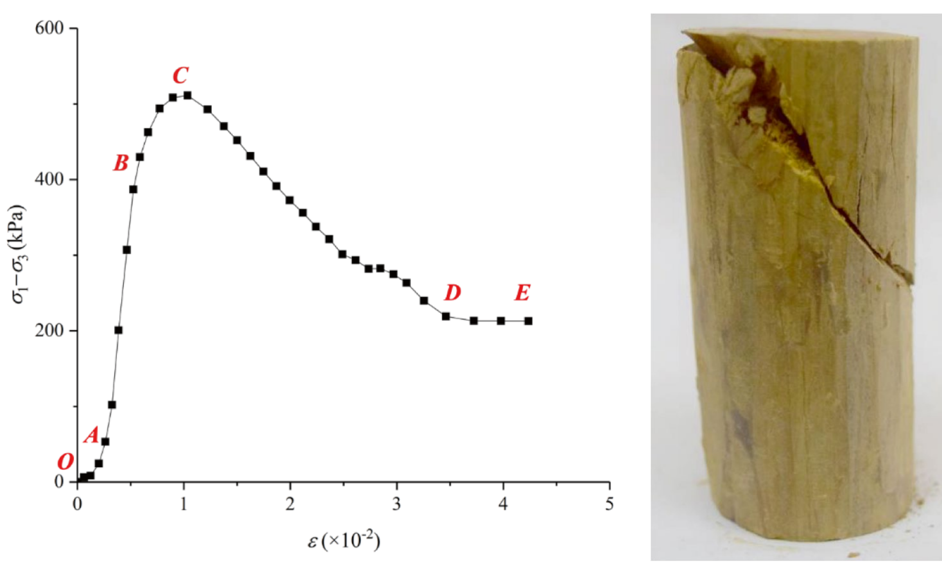

(a) Stress-strain curve **(b)** Failure mode

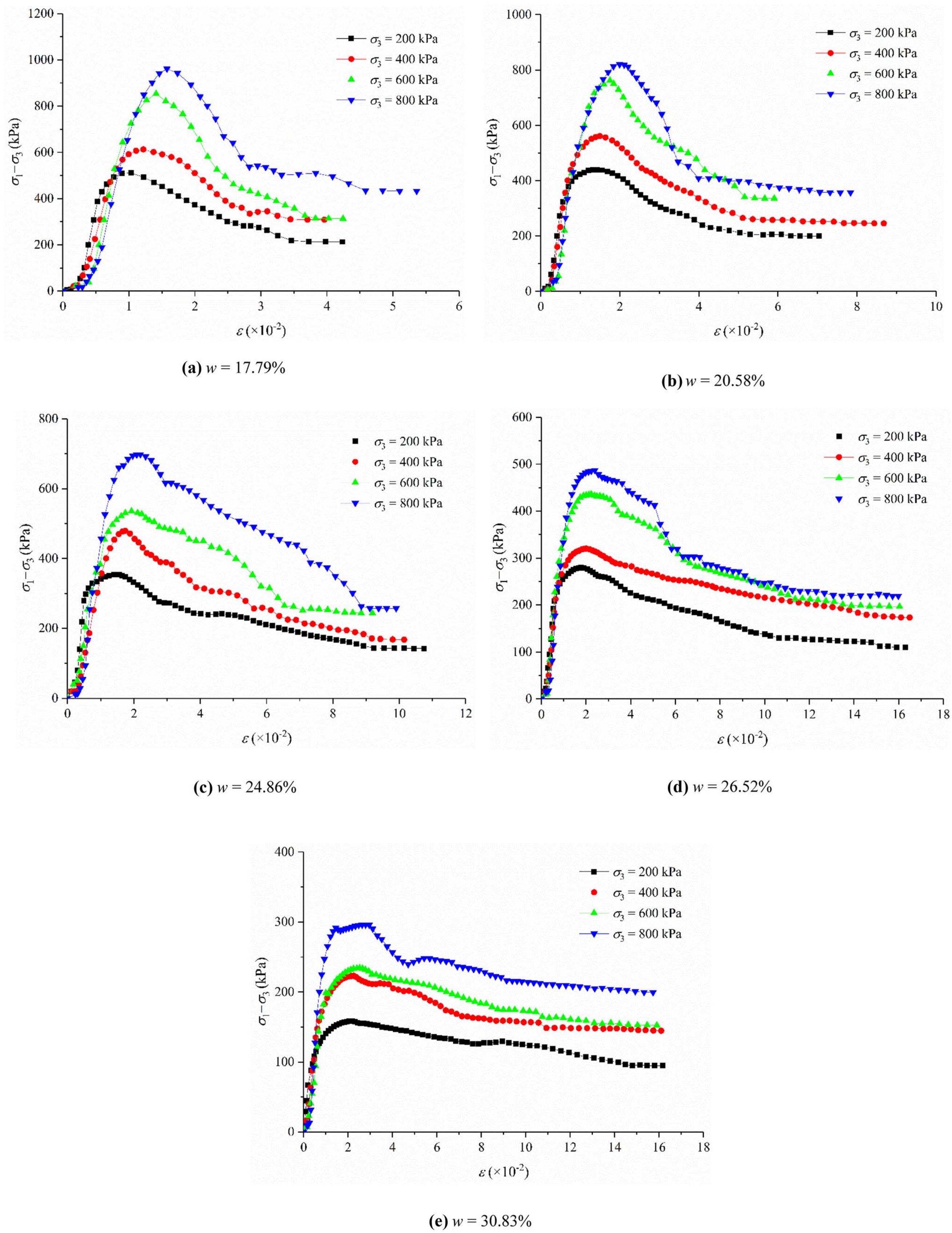

Fig. 10 Stress–strain curves of specimens with different water contents. **a** $w = 17.79\%$. **b** $w = 20.58\%$. **c** $w = 24.86\%$. **d** $w = 26.52\%$. **e** $w = 30.83\%$

Table 4 Axial strains corresponding to the peak strengths

w/%	$\varepsilon_f/\times 10^{-2}$			
	$\sigma_3=200$ kPa	$\sigma_3=400$ kPa	$\sigma_3=600$ kPa	$\sigma_3=800$ kPa
17.79	1.03	1.22	1.41	1.58
20.58	1.31	1.49	1.75	1.99
24.86	1.56	1.74	1.93	2.19
26.52	1.78	2.01	2.23	2.39
30.83	2	2.25	2.52	2.78

Average modulus

The average modulus was defined as the average slope of the approximate straight-line part of the stress–strain curve, and can be calculated as follows:

$$E_a = \frac{\sigma_{0.8} - \sigma_{0.2}}{\varepsilon_{L0.8} - \varepsilon_{L0.2}} \quad (3)$$

where $\sigma_{0.8}$ and $\sigma_{0.2}$ are 0.8 times and 0.2 times of the peak strength, respectively; $\varepsilon_{L0.8}$ and $\varepsilon_{L0.2}$ are the axial strains corresponding to $\sigma_{0.8}$ and $\sigma_{0.2}$, respectively.

Figure 12 shows the relationship between the average modulus of Xigeda formation and the confining pressure. When $w<26.52\%$, the correlation between the average modulus and the confining pressure is not obvious. When $w \geq 26.52\%$, the average modulus increases linearly with the raise of confining pressure, i.e., $w=30.83\%$, when the confining pressure raises from 200 to 800 kPa, the average modulus increases from 15.95 to 34.32 MPa. From the micro perspective, the reasons can be considered as follows. Under the condition of low water content, the cementation

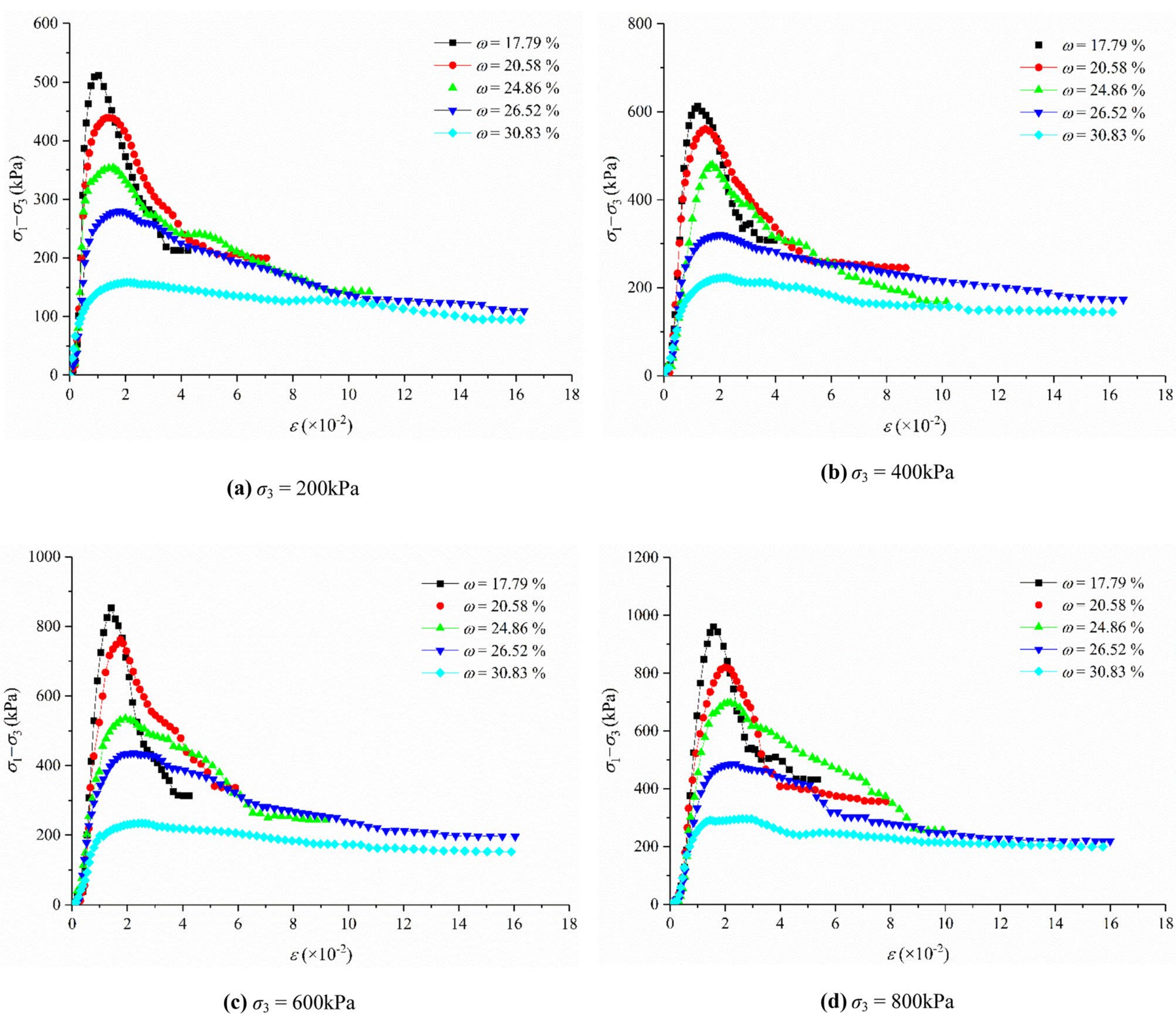

Fig. 11 Stress–strain curves under different confining pressures. **a** $\sigma_3=200$ kPa. **b** $\sigma_3=400$ kPa. **c** $\sigma_3=600$ kPa. **d** $\sigma_3=800$ kPa

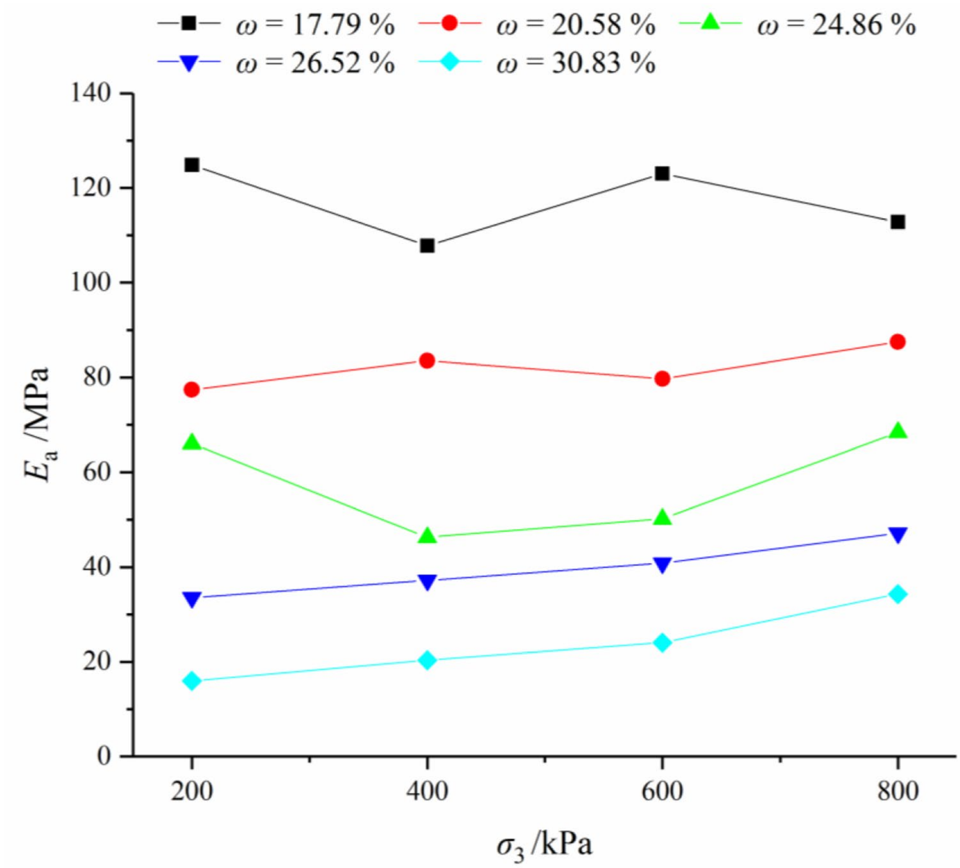

Fig. 12 Relationship between the average modulus and the confining pressure

between mineral particles is strong, the initial compaction degree of pores or fractures is low when the confining pressure is applied, and the secondary compaction degree of pores or fractures is less affected by the confining pressure in the process of deviatoric stress application, which makes the correlation between average modulus and confining pressure less obvious. Under the condition of high water content, the cementation between mineral particles is destroyed. During the process of confining pressure application, mineral particles are easy to slide and adjust their position. The initial compaction degree of pores and fractures is high, which results in the secondary compaction degree of pores and fractures affected by the confining pressure greatly in the process of deviatoric stress application, and the average modulus increases with the raise of confining pressure.

Figure 13 shows the relationship between the average modulus of Xigeda formation and the water content. Under certain confining pressure, the average modulus decreases approximately linearly with the raise of water content, i.e., when the confining pressure is 200 kPa, the water content increases from 17.79 to 30.83%, and the average modulus decreases from 124.81 to 15.95 MPa. From the micro perspective, the reasons can be considered as follows. The hygroscopic expansion of illite and montmorillonite produces the swelling force, which destroys the cemented structure and generates new pores or fractures. The free water enters the grain and forms a water film, which plays a certain role of lubrication. When the deviatoric stress is applied, the pores or fractures are easy to be compacted. The higher the water content is, the stronger the cemented structure is destroyed, and the compaction effect of pores or fractures is more obvious, which makes the average modulus decreases with the raise of water content.

Shear strength

Using the triaxial test data in Tables 2 and 3, in σ-τ space, the Mohr's circles of stress at peak strength and residual strength at different water contents were plotted. As shown in Figs. 14 and 15, in the range of tested conditions ($w = 17.79 \sim 30.83\%$, $\sigma_3 = 200 \sim 800$ kPa), both the peak and residual strengths meet the Mohr–Coulomb criterion. As shown in Table 5, the peak and residual shear strength indices at different water contents were obtained, where c and φ are the cohesion and friction angles, respectively, and the subscripts f and r represent the peak and residual values, respectively. The relationships among the shear strength indices including c_f, φ_f, c_r, and φ_r and the water content are illustrated in

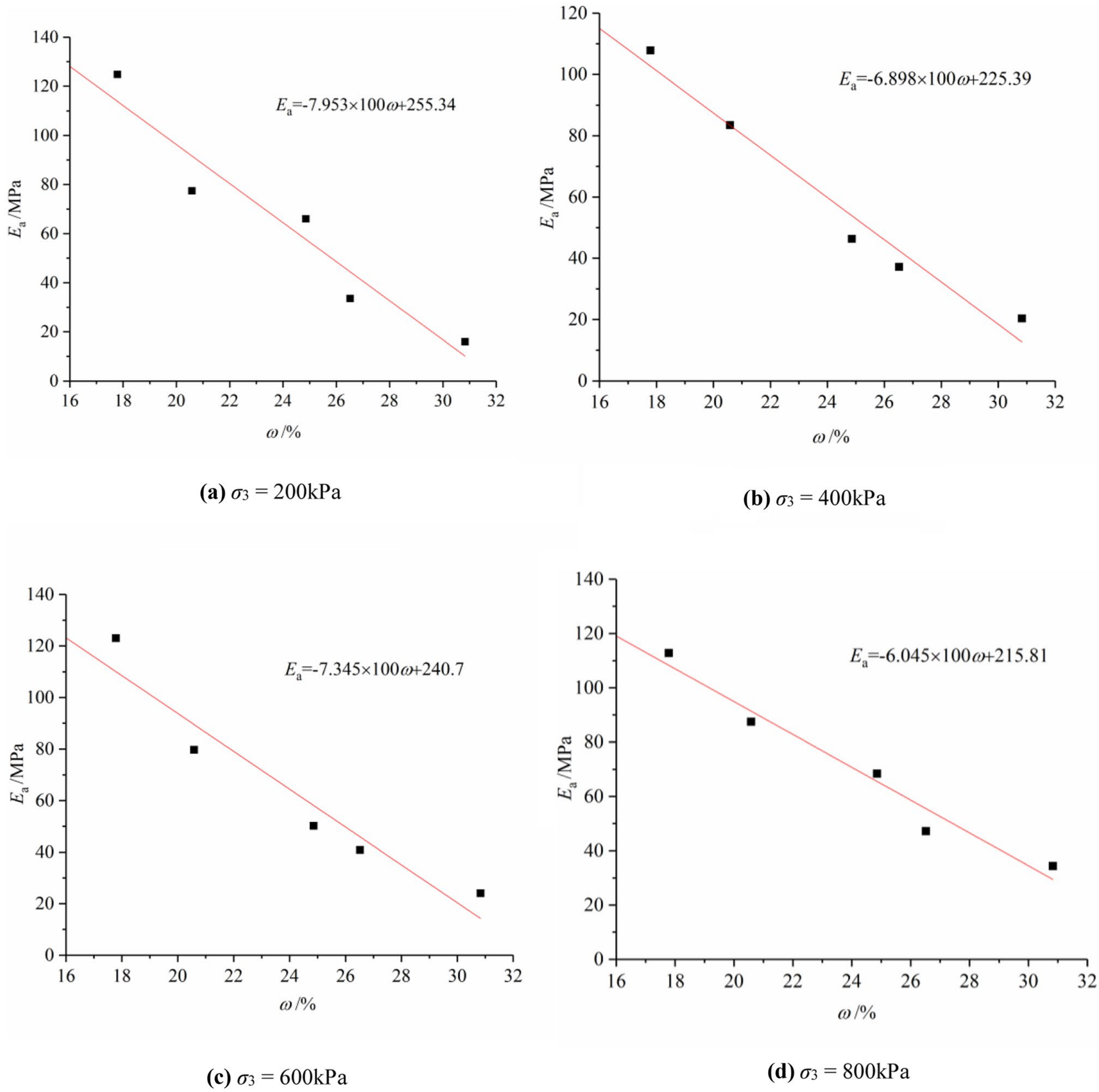

Fig. 13 Relationship between the average modulus and the water content. **a** $\sigma_3 = 200$ kPa. **b** $\sigma_3 = 400$ kPa. **c** $\sigma_3 = 600$ kPa. **d** $\sigma_3 = 800$ kPa

Fig. 16, which shows that c_f, φ_f, c_r, and φ_r decrease with increasing water content. For example, as the water content is increased from 17.79 to 30.83%, c_f is decreased from 126 to 55 kPa (a reduction of 56%); φ_f is decreased from 16.5 to 5.5° (a reduction of 67%); c_r is decreased from 65 to 33 kPa (a reduction of around 50%); φ_r is decreased from 8.2 to 4.3° (a reduction of 48%). According to the microstructure, the influence of water content on cohesion is mainly due to the chemical reaction of water with illite and montmorillonite. Absorption of the water molecules leads to the increase of the clay aggregate volume, generating expansive forces, and the cementation structure is thereby destroyed. The influence of water content on friction angle is mainly due to the water film between the particles and molecular forces, which tends to round the surface outline of the particles, and the lubricating effect of the water film itself.

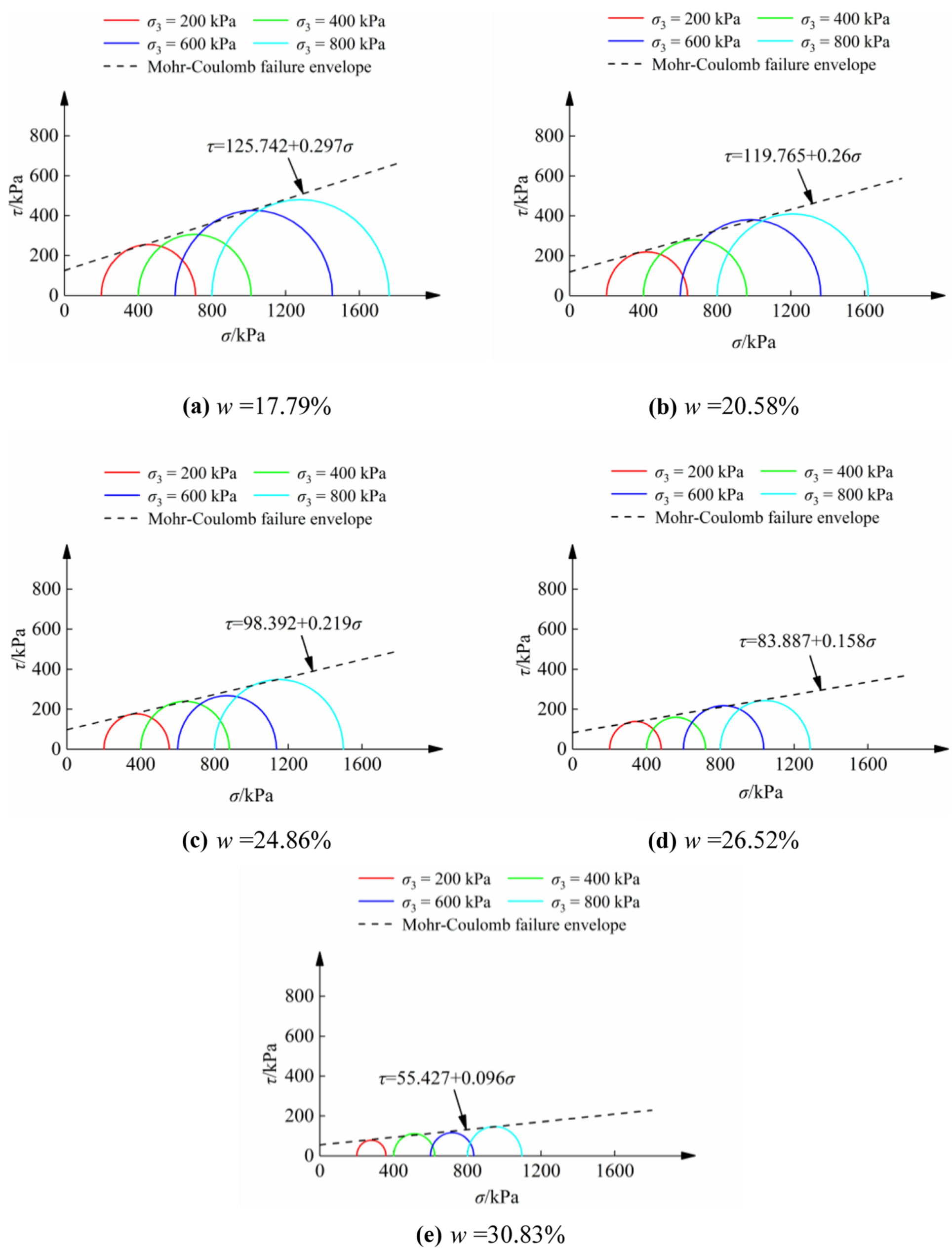

Fig. 14 Peak strength Mohr–Coulomb envelopes under different water contents. **a** $w=17.79\%$. **b** $w=20.58\%$. **c** $w=24.86\%$. **d** $w=26.52\%$. **e** $w=30.83\%$

It is noted that the cohesion of saturated Xigeda formation specimens is non-zero (Figs. 14 and 15), differing from the strength characteristics of most soils. During the test, although the strength of specimens sampled from the Xigeda formation deteriorated with increasing water content, they maintained their integrity in a manner similar to rock in its saturated state; moreover, the stress–strain curves of specimens sampled from the Xigeda formation may still show softening characteristics, unlike most soils that undergo strain hardening; thus, the weak cemented structure of the material in the Xigeda formation cannot be completely destroyed, even upon full saturation, and the cohesion will not be zero.

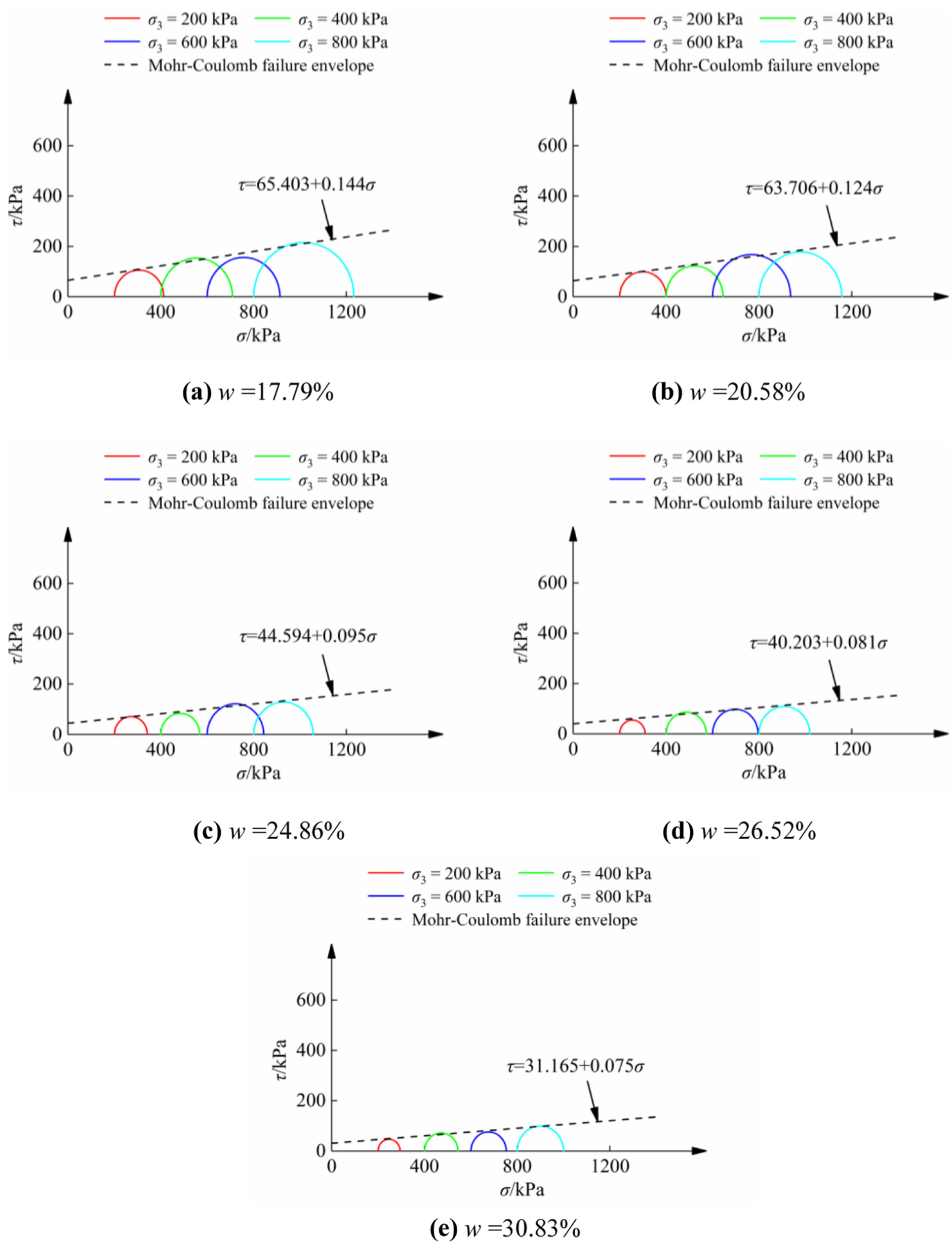

Fig. 15 Residual strength Mohr–Coulomb envelopes under different water contents. **a** $w = 17.79\%$. **b** $w = 20.58\%$. **c** $w = 24.86\%$. **d** $w = 26.52\%$. **e** $w = 30.83\%$

Table 5 Peak and residual shear strength indices with different water contents

w/%	c_f/kPa	φ_f/(°)	c_r/kPa	φ_r/(°)
17.79	125.74	16.53	65.4	8.18
20.58	119.77	14.57	63.71	7.07
24.86	98.39	12.36	44.59	5.44
26.52	83.89	8.96	40.2	4.62
30.83	55.43	5.50	31.17	4.28

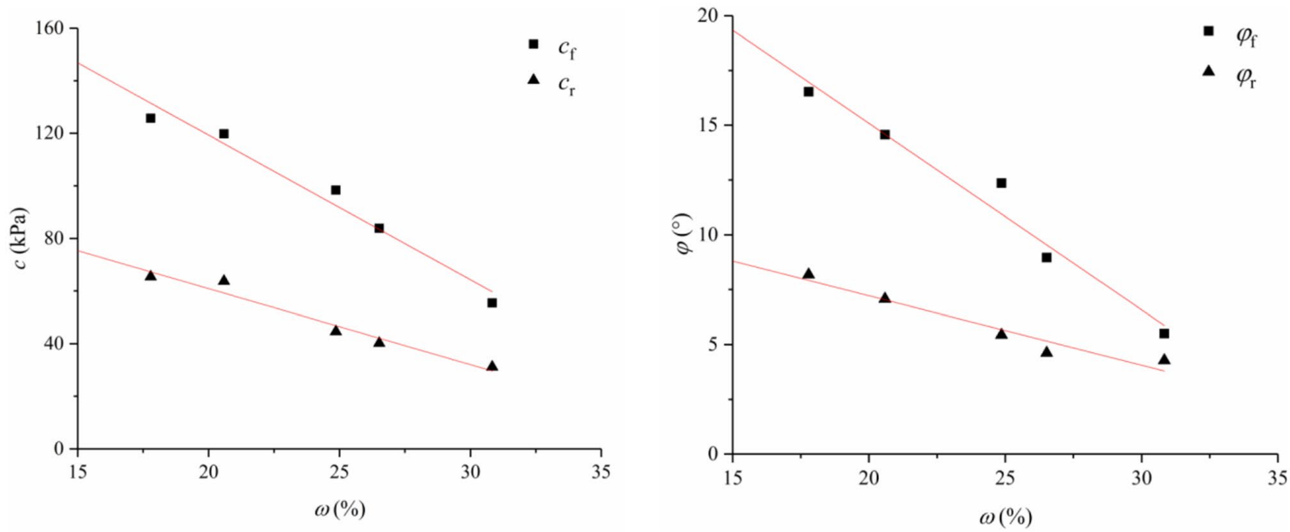

(a) c_f, c_r and w

(b) φ_f, φ_r and w

Fig. 16 Relationships between the shear strength indices and the water content. **a** c_f, c_r, and w. **b** φ_f, φ_r, and w

Conclusions

The Xigeda Formation in south-western China is a typical hard soil and soft/weak rock formation: the physico-mechanical behavior of the Xigeda formation is very sensitive to changes in water content. Specimens sampled from Zhaizi village along the Jinsha River have been tested to investigate the influence of water on the mechanical behavior of the Xigeda Formation. Through the XRD, SEM, and triaxial compression testing, the influences of water on both microstructure and mechanical behavior were investigated, and the relationships between the peak/residual strength and the water content were discussed. The main conclusions were as follows:

(a) The Xigeda formation is mainly composed of quartz, illite, montmorillonite, clinochlore, and other minerals. The Xigeda formation has the characteristics of a weakly-cemented structure, differing from that of soil or rock. Upon saturation, the number and extent of pores/fractures between particles increase, and the initial cementation is easily damaged, thus loosening the material.

(b) The stress–strain curve of the Xigeda formation can be divided into five stages. The deformation characteristics of the Xigeda formation are significantly affected by water content. With increasing water content, the gradients of the stress–strain curve in the elastic deformation stage decrease, while the axial strains corresponding to the peak strengths increase. Besides, the average modulus decreases approximately linearly with the raise of water content.

(c) The influence of water content on peak strength is much greater than that on residual strength, which means that the weakening ability of the water to the degree of cementation of a specimen is much greater than that of the roughness of the mineral contact surface or the roundness of mineral particles. When the water content is low, the peak strength drops rapidly to the residual strength, which shows the softening characteristics of a rock. When the water content is high, the gradients of the stress–strain curve after the peak strength are shallow, and the softening becomes less pronounced, typifying the deformation characteristics of a soil.

(d) In the range of tested conditions ($w = 17.79 \sim 30.83\%$, $\sigma_3 = 200 \sim 800$ kPa), both the peak strength and the residual strength meet the Mohr–Coulomb criterion. The shear strength indices including c_f, φ_f, c_r, and φ_r decrease with increasing water content, which is caused by the chemical reaction of water with illite and montmorillonite. Specifically, as the water content increases from 17.79 to 30.83%, c_f decreases from 126 to 55 kPa, φ_f decreases from 17 to 5.5°, c_r decreases from 65 to 33 kPa, and φ_r decreases from 8.2 to 4.3°.

Funding The work reported in this paper is financially supported by the Youth Innovation Promotion Association CAS (No. 2021325), the National Natural Science Foundation of China (No. 52179117), and the International Partnership Program of Chinese Academy of Sciences Grant No. 131551KYSB20180042.

References

Abolmasov B, Milenković S, Marjanović M, Đurić U, Jelisavac B (2014) A geotechnical model of the Umka landslide with reference to landslides in weathered Neogene marls in Serbia. Landslides 12(4):689–702

Alonso EE, Pinyol NM (2014) Slope stability in slightly fissured claystones and marls. Landslides 12(4):643–656

Aversa S, Evangelista A (1998) The mechanical behaviour of a pyroclastic rock: yield strength and destructuration effects. Rock Mech Rock Eng 31(1):25–42

Barla G, Barbero M, Castelletto M, Maderni G (1998) A case of plane shear slope instability during the severe rainfall event of 4–6 November 1994 in Piemonte (Italy). 2nd International Symposium on Hard Soils and Soft Rocks, Naples (Italy), 12–14 October 1998

Cecconi M, Viggiani GM (2001) Structural features and mechanical behaviour of a pyroclastic weak rock. Int J Numer Anal Meth Geomech 25(15):1525–1557

Clayton CRI, Serratrice JF (1993) The mechanical properties and behaviour of hard soils and soft rocks. Proceedings of the International Symposium on Geotechnical Engineering of Hard Soils and Soft Rocks, Athens 3:1839–1877

Corominas J, Martínez-Bofill J, Soler A (2014) A textural classification of argillaceous rocks and their durability. Landslides 12(4):669–687

Di Maio C, Scaringi G, Vassallo R (2014) Residual strength and creep behaviour on the slip surface of specimens of a landslide in marine origin clay shales: influence of pore fluid composition. Landslides 12(4):657–667

Gens A, Nova R (1993) Conceptual bases for a constitutive model for bonded soils and weak rocks. Proceedings of the International Symposium on Geotechnical Engineering of Hard Soils and Soft Rocks. Athens 1:447–455

Gens A, Vaunat J, Garitte B (2005) Elastoplastic modelling of hard soils and soft rocks: formulation and application. VIII Int. Conf. Computational Plasticity, COMPLAS VIII, Barcelona

Hornig ED, Klapperich H (2011) Laboratory tests and field measurements investigating the stress strain behaviour of foundations on hard soil and weak rock. In: Anagnostopoulos A, Pachakis M, Tsatsanifos C (eds) Geotechnics of hard soils-weak rocks: Proceedings of the 15th European conference on soil mechanics and geotechnical engineering. IOS Press, Athens, Greece, pp 737–742

Kanji MA (2014) Critical issues in soft rocks. J Rock Mech Geotech Eng 6(3):186–195

Kavvadas M, Amorosi A (2000) Constitutive models for structured soils. Geotechnique 50(3):263–273

Kong P, Granger DE, Wu FY, Caffee MW, Wang YJ, Zhao XT, Zheng Y (2009) Cosmogenic nuclide burial ages and provenance of the Xigeda paleo-lake: implications for evolution of the Middle Yangtze River. Earth Planet Sci Lett 278:131–141

Li P, Liu XS, Yang ME, Yuan JL (2012) Analysis of generation factors for tectonic deformation, in the Xigeda formation in southwestern China. Analysis of generation factors for tectonic deformation in the Xigeda formation in southwestern China. Eng Sci 10(1):8–13

Ling S, Wu X, Liao X, Li X, Zhao S (2015) Study on the water-rock interaction behavior of Xigeda strata in Lamaxi Gully, Sichuan Province, China. In: Lollino G et al (eds) Engineering Geology for Society and Territory -, vol 2. Springer, Cham, pp 2107–2111

Liu HJ, Nie DX (2004) A summary of the study of Xigeda Strata. Adv Earth Sci 19:80–82. (In Chinese with English Abstract)

McCammon N (1999) Book review: The geotechnics of hard soils-soft rocks. Can Geotech J 36(6):1206–1206

Moon VG (1993) Geotechnical characteristics of ignimbrite: a soft pyroclastic rock type. Eng Geol 35(1–2):33–48

Picarelli L (2015) Landslides in hard soils and weak rocks. Landslides 12(4):641–641

Quaternary Glacier Survey Group (1977) Preliminary study on Xigeda formation in southwest China. In: Institute of Geomechanics, Chinese Academy of Geological Sciences (ed) Collection on Quaternary Glacial Geology of China. Geological Publishing House, Beijing, pp 144–154. (In Chinese)

Rotaru A (2011) Landslides triggered in hard soils and soft rocks in Romania. In: Anagnostopoulos A, Pachakis M, Tsatsanifos C (eds) Geotechnics of hard soils-weak rocks: Proceedings of the 15th European conference on soil mechanics and geotechnical engineering. IOS Press, Athens, Greece, pp 1383–1388

Shao JF (1998) Poroelastic behaviour of brittle rock materials with anisotropic damage. Mech Mater 30:41–53

Shang T (2012) Research on micro-characteristic of CH8 oil reservoir of Yanchang formation in HuaQing area of the Ordos Basin. Northwest University. (In Chinese)

Sitarenios P, Bardanis M, Kavvadas M (2011) Modelling the soil-water characteristic curve of structured and recomposed hard soils-weak rocks. In: Anagnostopoulos A, Pachakis M, Tsatsanifos C (eds) Geotechnics of hard soils-weak rocks: Proceedings of the 15th European conference on soil mechanics and geotechnical engineering. IOS Press, Athens, Greece, pp 665–670

Sun ZF, Qu HL, Wu XX (2012) Research on the axial load transmission function of cast-in-place pile in Xigeda rock stratum. Adv Mat Res 594–597:612–615

Tatsuoka F, Kohata Y (1995) Stiffness of hard soils and soft rocks in engineering applications. Proc. 1st Int. Symp Prefailure Deformation Characteristics of Geomaterials, Sapporo 2:947–1063

Tommasi P, Verrucci L, Rotonda T (2014) Mechanical properties of a weak pyroclastic rock and their relationship with microstructure. Can Geotech J 52(2):1–13

Vaughan PR (1993) Engineering behavior of weak rocks: some answers and some questions. Proceedings of the International Symposium on Geotechnical Engineering of Hard Soils and Soft Rocks, Athens 3:1741–1765

Vukadin V (2007) Modeling of the stress-strain behavior in hard soils and soft rocks. Acta Geotechnica Slovenica 2(2):5–15

Wang W, Chen W, Long W, Die J (2018) Research and analysis on the landslide characteristics of Xigeda soil slope. American Institute of Physics Conference Series. American Institute of Physics Conference Series. AIP Conference Proceedings 1944, 020012

Xu ZM (2011) Deposits of Zhaizi village landslide-dammed lake along Jinsha River and its implication for the genesis of Xigeda Formation. Geogr Rev 57(5):675–686. (In Chinese with English Abstract)

Xu ZM, Liu WL (2011) Some problems in the study of the genesis of Xigeda Formation. Earth Sci Front 18(5):256–270 (In Chinese with English Abstract)

Yang SH, Su LJ, Zhang CL, Li C, Hu BL (2020) Analysis of seepage characteristics and stability of Xigeda Formation slope under heavy rainfall. Journal of Civil and Environmental Engineering. http://kns.cnki.net/kcms/detail/50.1218.TU.20200224.1823.004.html. (In Chinese with English Abstract)

Yuan FL (1958) Some stratigraphical material from southwestern area. China Quaternaria Sinica 1(2):130–140 (In Chinese)

Zhang S (2009) Geological formation names of China (1866–2000). Springer, pp 1250

Zhang YS, Qu YX (2000) Definition of hard soil-soft rock and its discrimination and classification. Geological Science and Technology Information 19(1):77–80. (In Chinese with English Abstract)

Zhou P, Wang ZJ, Xu HY, Zhao QC, Sun CS (2017) Stability and sub-classification study on the tunnel surrounding rock of Xigeda strata considering the influence of moisture content. Chin Civil Eng J 50(12):97–110 (In Chinese with English Abstract)

Zhou LG (2016) Research on the microscopic features and mechanical properties of silty sands used in subgrade in seasonally frozen region. Jilin Jianzhu University. (In Chinese)

Zimbardo M, Cannone C, Ercoli L, Nocilla A (2018) A risk assessment proposal for underground cavities in Hard Soils-Soft Rocks. Int J Rock Mech Min Sci 103:43–54